Environmental Research 292 (2026) 123661

Contents lists available at ScienceDirect

Environmental Research

journal homepage: www.elsevier.com/locate/envres

Immune profiling of human blood cells after indirect exposure to crystalline silica particles

Evangel Kummari [a], Anja Bråthen Kristoffersen [b], Sabin Bhandari [b], Hege Hjertholm [a], Hubert Dirven [a], Sarah E. Josefsson [a], François Huaux [c], Riccardo Leinardi [c], Cristina Pavan [c,d], Manosij Ghosh [e], Peter Hoet [e], Unni C. Nygaard [b], Birgitte Lindeman [a,*]

[a] Division of Climate and Environmental Health, Norwegian Institute of Public Health, Oslo, Norway
[b] Division for Infection Control, Norwegian Institute of Public Health, Oslo, Norway
[c] Louvain Centre for Toxicology and Applied Pharmacology, Université Catholique de Louvain, Brussels, Belgium
[d] Department of Chemistry and "G. Scansetti" Interdepartmental Centre for Studies on Asbestos and Other Toxic Particulates, University of Turin, Turin, Italy
[e] Department of Public Health and Primary Care, Environment and Health, KU Leuven, Belgium

ARTICLE INFO

Keywords:
Respirable crystalline silica (RCS)
Immune cell profiling
Macrophages
Whole blood
ex vivo

ABSTRACT

Occupational exposure to respirable crystalline silica (RCS) is a significant health concern associated with pulmonary and systemic diseases, mediated in part through lung macrophage toxicity. In this study, we employed an *ex vivo* indirect exposure model, to explore potential links between silica-induced macrophage toxicity and changes in innate and adaptive immune cell phenotypes, that may contribute to systemic effects of RCS. THP-1 derived macrophages served as a macrophage model and were exposed to crystalline silica particles. Whole blood was subsequently exposed *ex vivo* to conditioned medium (CM) from these particle-exposed cells. We then characterized immune cell responses via soluble cytokine analysis and single cell profiling by mass cytometry. Two crystalline silica types were compared, Min-U-Sil 5 quartz (Minusil) and synthetic quartz (gQ), that differ in "nearly free silanols" (NFS)—functional groups linked to RCS pathogenicity. In one set of experiments, an immune stimulation cocktail was added during the last 4 h of exposure to observe potential Minusil-induced changes in cellular immune responses. The findings demonstrated that exposing whole blood to Minusil CM significantly elevated soluble pro-inflammatory cytokines levels. At the single cell level, Minusil CM exposure altered monocyte and dendritic cell subpopulation frequencies and increased frequencies of several lymphocyte populations with high expression of the early activation marker CD38. Following immune stimulation, two cytotoxic effector memory T cell subpopulations showed increased frequencies: one polyfunctional and one characterised by a high expression of CD161. This study provides novel data on immune cell profiles associated with *ex vivo* exposure to RCS.

1. Introduction

Crystalline silica is a major component of sand and rocks, with quartz being the most common polymorph found in nature (Uhrlandt, 2006; Atsdr, 2019). Respirable particles are defined as the mass fraction of inhaled particles that penetrate to the unciliated airways (Brown et al., 2013), generally considered to be particles with a mass median aerodynamic diameter (MMAD) of 4 μm or below (Jrc, 2002). Occupational exposure to respirable crystalline silica (RCS) can occur during various processes such as mining, sandblasting and ceramics production. More recent sources of exposure include processes such as denim sandblasting and artificial stone benchtop fabrication (Barnes et al., 2019).

Exposure to RCS is associated with lung diseases, including silicosis, fibrosis, and lung cancer (Hoy and Chambers, 2020), as well as an increased risk of systemic diseases such as cardiovascular disease (Miyata and Van Eeden, 2011; Gurzu et al., 2025). Additionally, RCS is one of the few environmental factors clearly associated to an increased risk of developing human autoimmune diseases such as systemic sclerosis, rheumatoid arthritis, and systemic lupus erythematosus (Miller et al., 2012; Pollard, 2020; Fireman and Fireman Klein, 2024). Although occupational exposure to RCS has been reduced over the years, it continues to pose a significant global health concern (Chen et al., 2022;

* Corresponding author.
E-mail address: birgitte.lindeman@fhi.no (B. Lindeman).

https://doi.org/10.1016/j.envres.2025.123661
Received 10 July 2025; Received in revised form 30 November 2025; Accepted 29 December 2025
Available online 29 December 2025

Delabre et al., 2023; Liu et al., 2023; Decos, 2024). Crystalline silica remains the primary cause of occupational respiratory diseases worldwide (Cullinan et al., 2017). Millions of workers are exposed to RCS due to emerging sources of exposure or insufficient preventative measures (Hoy and Chambers, 2020; Fazio et al., 2025). According to the Global Burden of Disease Study, silicosis was in 2017 responsible for over 10, 000 deaths and more than 200,000 years of life lost (GBD, 2017). RCS exposure concentrations can vary by up to three to four orders of magnitude and may exceed occupational exposure limits in some industries (Decos, 2024) and during specific operations (Ronsmans et al., 2022). Current occupational exposure limits (OELs) for RCS, given as 8-h time-weighted average, are generally around 0.05–0.1 mg/m^3, whereas the low-risk and high-risk lung cancer risk estimates provided by the recent joint DECOS and Nordic Exposure Group report were 0.00038 mg/m3 and 0.0363 mg/m3, respectively (Decos, 2024).

Inhaled RCS reaches deep into the lungs, where the particles are phagocytosed by alveolar macrophages, leading to phagolysosomal membrane destabilisation, inflammasome activation and cell death (Leung et al., 2012; Leinardi et al., 2020). RCS is cleared slowly from the lungs, inducing repeated cycles of phagocytosis followed by oxidative stress, inflammation, epithelial barrier damage and cell death (Vallyathan et al., 1988; Castranova, 1994; Leinardi et al., 2022). Chemical analysis of lung biopsies from silicosis patients using X-ray fluorescence revealed an average silica level of about 7000 ppm, 5- to 10-fold higher than in tissue from patients with idiopathic pulmonary fibrosis (Fireman et al., 2021).

The cycle of particle phagocytosis and macrophage death results in prolonged lung inflammation (Pavan and Fubini, 2017; Pavan et al., 2024) and may also trigger a systemic inflammatory response (Miyata and Van Eeden, 2011). Stressed and damaged macrophages release proinflammatory mediators and damage-associated molecular patterns (DAMPs) that elicit innate and adaptive immune responses, including presentation of self-antigens to lymphocytes (Pollard, 2020; Huang et al., 2021; Leinardi et al., 2022; Qin et al., 2024).

Although RCS particle toxicity has been much studied, there is a scarcity of data characterising potential changes in circulating immune cells that may link silica exposure to systemic disease risk. We hypothesize that RCS-induced macrophage toxicity and proinflammatory signalling, may indirectly influence the activation and phenotypic characteristics of innate and adaptive peripheral immune cells.

In this study, we have exposed model macrophages to two types of α-quartz particles: the commercial quartz Min-U-Sil 5 (hereafter referred to as Minusil) and synthetic as grown quartz (gQ particles) (Pastero et al., 2016). Minusil is widely used as model particle for studies of crystalline silica induced toxicity. The two particle types exhibit different characteristics, as Minusil has fractured surfaces rich in reactive “nearly free silanols” (NFS), whereas the gQ particles have an unfractured, NFS-poor surface (Pavan et al., 2020, 2024). Fractured surfaces typically result from mechanical comminution of quartz rocks, a process common in various occupational settings, including mining, milling, cutting, sandblasting, and polishing (Donaldson and Borm, 1998; Gobindlal et al., 2021). These fractured surfaces are highly reactive and, upon exposure to environmental moisture, form more stable silanol groups (i.e., –SiOH) (Bellomo et al., 2024). NFS are silanol groups arranged at a specific interatomic distance (approximately 4–6 Å) and are found on the surface of inflammogenic and fibrogenic quartz particles obtained by fracturing, including Minusil (Pavan et al., 2020, 2024). In contrast, synthetic quartz crystals, characterized by smooth, unfractured surfaces, exhibit significantly lower NFS content and were found to be non-inflammogenic (Pavan et al., 2020, 2024). The presence of NFS has been positively associated with membranolytic activity in model systems (Pavan et al., 2022, 2023), macrophage activation and pro-inflammatory responses (Leinardi et al., 2020, 2023), and adverse lung outcomes including acute and chronic inflammation, fibrosis, lung cancer, and autoimmune responses *in vivo* (Pavan et al., 2020, 2024). In a recent study, we showed a redistribution of Minusil to extrapulmonary sites during the first three days after which the level stabilised at slightly more that 50 % of deposited amount for a period up to 4 months (Leinardi et al., 2025). In contrast the NFS-poor gQ particles remained in the lung, likely reflecting Minusil-induced toxicity leading to impaired alveolar-capillary barrier integrity (Leinardi et al., 2025).

Whole blood from multiple healthy donors was exposed *ex vivo* to CM harvested from RCS-exposed macrophage-like cells. Whole blood was chosen as it represents a test matrix with high physiological relevance. We subsequently characterized changes in immune cell profiles using high-dimensional single-cell profiling by mass cytometry and multiplex cytokine profiling to assess the complexity of circulating immune cell subtypes and function. By employing this indirect exposure model, we provide new data on putative links between RCS-induced macrophage-like cell toxicity and modulation of innate and adaptive immune cells.

2. Materials and methods

2.1. Study design

THP-1 derived macrophage-like cells constitute a well-characterized human macrophage model widely used for studies of particle toxicity (Chanput et al., 2014; Ruijter et al., 2025). THP-1 derived macrophage-like cells were exposed for 24 h to two RCS particles differing in their surface characteristics (NFS). Cell viability and cytokine levels in the culture medium were measured. For the secondary exposure model, CM from the macrophage-like cells was collected and incubated with human whole blood in a 1:1 ratio for 24 and 48 h (Fig. 1). The CM consists of signalling molecules and DAMPs released from stressed and dying cells. Human whole blood was used as it represents a biological relevant exposure matrix suitable to determine immune responses to cytokines and DAMPs. Two sets of experiments were performed. In the first one, whole blood soluble cytokines were characterised at 24 and 48 h, and single cell immune profiling was performed after 48 h of exposure. IL-1β was used as a positive control, mimicking inflammasome activation. In a second experimental setup, the blood cells were further stimulated with an immune stimulation cocktail, to assess functional changes after secondary exposure to Minusil particles.

2.2. Crystalline silica particles

Crystalline silica particles (Min-U-Sil®5 ground quartz) were from U. S. Silica Company [Berkeley Springs, WV, USA]. Synthetic, as-grown α-quartz (gQ) particles with a quasi-perfect crystal habit were synthesised at the “G. Scansetti Centre” (University of Torino, Italy) (Pastero et al., 2016; Leinardi et al., 2020). In contrast to Minusil particles, the gQ particles have an unfractured surface and are devoid of NSF groups, which have been linked to cytotoxic and inflammatory responses (Pavan et al., 2020). Main characteristics of the two quartz particles are summarized in Supplementary Table S1, based on deep characterization in previous studies (Leinardi et al., 2020; Skuland et al., 2020a; Pavan et al., 2023) and characterisation of the Minusil particles to add missing data for the specific batch used. Minusil endotoxin content was measured by the Pierce Chromogen Endotoxin Quant kit (LAL-method) and showed low level of contamination 0.01 EU/ml for Min-U-Sil (Skuland et al., 2020b). The gQ particles were not tested for endotoxin and we thus cannot not exclude some level of contamination, although the cytokine data show a very low pro-inflammatory activity of these particles.

2.3. THP-1 cell culture

THP-1 cells (human acute monocytic leukemia cell line) were obtained from the American Type Culture Collection [Manassas, VA, USA]. The cells were maintained at 37 °C (95 % room air, 5 % CO2) in cell culture media (RPMI-1640 Glutamax™ [Gibco, Thermo Fischer

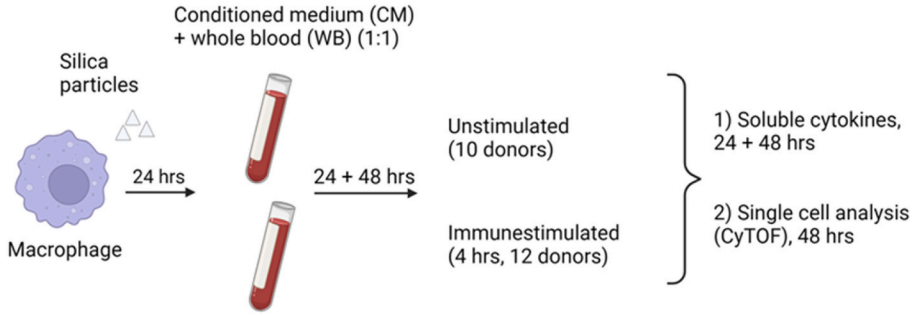

Fig. 1. Study Design for the Secondary Exposure Model. THP-1 derived macrophage-like cells were exposed to crystalline silica (Minusil and gQ) for 24 h. The conditioned medium (CM) from this exposure was then used to incubate whole blood (WB) at a 1:1 ratio for 24 and 48 h. Soluble cytokines were analysed at 24 and 48 h by Luminex or Elisa, whereas single cells were analysed after 48 h using CyTOF. Created in BioRender.com.

Scientific, Waltham, MA, USA], supplemented with 1 mg/ml sodium pyruvate [Sigma-Aldrich, St. Louis, MO, USA], Hepes [Sigma-Aldrich, St. Louis, MO, USA], 0.09 % gentamicin [Gibco, Thermo Fischer Scientific, Waltham, MA, USA] and 10 % foetal calf serum [FCS; Biochrom, Berlin, Germany]) as previously described (Skuland et al., 2020a). For differentiation into macrophage-like cells, $1x10^6$ THP-1 cells per well were seeded in a 6-well plate with phorbol 12-myristate 13-acetate (PMA, 32 nM) for 24 h. The cells were subsequently cultivated for 72 h in PMA-free cell culture medium until exposure. Cell morphology and attachment to culture wells was in each experiment assessed visually by light microscopy (Supplementary Fig. S1).

2.4. Exposure of THP-1 derived macrophage-like cells and generation of conditioned medium (CM)

Dose-response analysis for Minusil particles with concentrations ranging from 0 to 300 μg/ml was performed and cell viability was measured by the Alamar Blue assay (data not shown). A concentration of 250 μg/ml was chosen for the further experiments to obtain a 30–50 % reduction of cell viability. A certain level of cell death was intended for the conditioned medium to present factors released from both live and dead cells. The same mass concentration of gQ particles were used. Uptake of Minusil and gQ particles in PMA-differentiated THP-1 macrophage-like cells has been demonstrated in a previous study (Leinardi et al., 2020). The cells were treated with silica particles in cell culture media for 24 h. Immediately prior to exposure, particles were suspended in serum-free culture medium, and bath sonicated for 15 min before use. The controls were exposed to similar treated cell culture medium without particles. After exposure, cells and cell debris were removed by centrifugation (300×*g* for 10 min at 4 °C), followed by a second centrifugation (10,000×*g* for 10 min at 4 °C) to remove particles. This freshly prepared CM was used for secondary exposure of whole blood, and the remaining supernatant was frozen for later analysis of LDH and cytokine levels.

2.5. Exposure of whole blood to conditioned medium (CM)

Male and female blood donors, aged 32–56 years, were recruited among healthy employees at the Norwegian Institute of Public Health, none of whom had any known immune or allergic diseases. This study was approved by the Norwegian Regional Committees for Medical and Health Research Ethics, and all donors signed an informed consent (REK, ID No 99836). Venous blood (approximately 10 ml) was collected from the volunteers into a sodium-heparin BD Vacutainer tube and immediately used for exposure to fresh macrophage CM.

2.5.1. Exposure of whole blood to CM

In the first of two sets of experiments, CM from control, Minusil and gQ exposed macrophage-like cells were incubated with whole blood at a 1:1 ratio (800 μl of each) in 5 ml polypropylene tubes for 24 and 48 h at 37 °C and 5 % CO_2 on a roller set to a low speed of 0.5 rpm. A total of 10 donors (5 Male/5 Female) were included. IL-1β (25 ng/ml in culture medium) was added to the whole blood at a 1:1 ratio in an additional experimental group to serve as a reference control for pro-inflammatory responses in the CyTOF analysis. IL-1β is secreted by macrophages exposed to crystalline silica particles and is considered a critical mediator of RCS-induced lung inflammation (Srivastava et al., 2002; Guo et al., 2013; Weng et al., 2015). Samples from the 48-h incubations were immediately processed for CyTOF analysis.

2.5.2. Exposure of whole blood to CM with an additional immune stimulation

To assess indirect effects of RCS on immune cell function, the second set of experiments included an immune stimulating cocktail. This experiment was performed only with Minusil particles, as these were the most potent. CM from unexposed (control) and Minusil exposed macrophages were incubated with whole blood for 48 h in a 1:1 ratio. For assessment of potential changes in cellular function, all samples were treated with a cocktail of immune stimulants during the final 4 h of the incubation period and then processed for CyTOF. The stimulation cocktail was designed to activate main innate and adaptive cell types and contain components relevant for viral and bacterial challenges (Poly (I:C), R848 and LPS) as well as primarily T cell activating PMA/Ionomycin. Whole blood from a total of 12 donors were exposed in this experiment with immune stimulation cocktail. Eight donors (4M/4F) were incubated with a stimulation cocktail containing R848–0.131 μg/ml; PMA - 0.008 μg/ml, Ionomycin - 0.667 μg/ml; LPS - 0.042 μg/ml; Poly I:C - 4.167 μg/ml (designated as “Low concentration”). An additional 4 donors (2M/2F) were incubated with a cocktail that was twice the concentration of the original cocktail (designated as “High concentration”) (R848–0.262 μg/ml; PMA - 0.016 μg/ml; Ionomycin - 1.334 μg/ml; LPS - 0.084 μg/ml; Poly I:C - 8.334 μg/ml to examine whether a stronger immune stimulation influenced the exposure-induced functional changes.

2.6. Cell viability and cytotoxicity measurements

As a measure of cell viability, macrophage metabolic activity was analysed by the Alamar Blue assay [Invitrogen by Thermo Fischer Scientific, Waltham, MA, USA], performed according to the manufacturer's instructions. Alamar blue solution was diluted 1:10 in serum-free cell culture medium and added to the cell culture at a volume of 1 ml per well. The cells were then incubated for 1 h at 37 °C at 5 % CO_2 environment. After incubation, 100 μl of the supernatant was transferred to a 96-well cell culture plate and fluorescence emission at 560/590 nm was measured using a CLARIOstar® plate reader [BMG LABTECH, Ortenberg, Germany]. Macrophage membrane integrity was measured in a lactate dehydrogenase (LDH) release assay. Measurements and

calculations were performed according to the manufacturer's guidelines [Roche, Germany] using a TECAN Sunrise plate reader [Männedorf, Switzerland] at 490 nm. Cell number and viability for whole blood samples were measured by a Count and viability assay [Muse Count&Viability kit, MCH 100102] on a MUSE cell counter before and after incubation with the CM. There was no consistent difference between treatments for the whole blood samples that showed mean % viability of >98 %, >90 % and >87 % at the 0-, 24- and 48-h timepoints, respectively. However, a reduction, especially of neutrophils, is expected during the 48 h culture period and is reflected in the reduced percentage of neutrophils at 48 h (Supplemental Figs. 5 and 6). Viability and cytotoxicity data are presented as % difference from control and statistical difference was tested by non-parametric comparisons using Steel method.

2.7. Measurements of inflammation markers in culture medium and blood

Cytokines and chemokines were measured by multi-plex analysis (Bio-Techne Luminex Human Discovery Assay) on a Bio-Plex reader (Bio-Rad, United Kingdom) for detecting fluorescence intensities. Eighteen analytes were measured (1-plex: Myeloperoxidase (MPO), 17-plex: CCL2/MCP-1, CCL3, CCL4/MIP-1 beta, CXCL2, CXCL10, GM-CSF, IFN-alpha (IFN-α), IFN-gamma (IFN-γ), IL-1beta (IL-1β), IL-4, IL-6, IL-8/CXCL8, IL-13, IL-17/IL-17A, IL-18, IL-23, TNF-alpha (TNFα)). All samples from the same experiment were measured on the same 96-well plate to avoid plate-to-plate variability. Bio-Plex Manager 6.1 software (RRID: SCR_014330, Bio-Rad, United Kingdom) was used to generate standard curves for determining concentrations of unknown samples. Total (latent and active) TGF- β1 concentrations were measured by ELISA (R&D Systems, USA), according to the manufacturer's instructions. For all statistical analyses of the Luminex measurements, the mean fluorescence intensity (MFI) values of soluble cytokines and chemokines were used and analysed with a linear mixed effect model with log [MFI] as outcome, donor and experiment as random effect and treatment as fixed effect. FDR adjusted p-values <0.1 were considered significant. In the summary tables for the unstimulated samples, cytokine concentrations are shown to facilitate comparisons of cytokine levels.

2.8. Immune cell profiling by mass cytometry (CyTOF)

CyTOF analysis was performed as previously reported (Sonnet et al., 2020; Nygaard et al., 2021) with adaption to whole blood instead of peripheral blood mononuclear cell (PMBC) and the use of barcoding procedures to minimize variations within each experiment. During the last 4 h of incubation of the whole blood, Brefeldin A (BFA) was added to inhibit protein secretion, while IdU was added to label proliferating cells. After incubation, the cells were resuspended in Cell - ID Cisplatin [Standard Biotools] for viability staining. Cells were washed and lysed to remove red blood cells, using the Cytodelics whole blood processing kit [Cytodelics AB, Sweden].

A total of eight samples from 2 donors (4 treatment groups per donor) and an internal reference sample were used for each experiment, and the samples were barcoded using Cell-ID 20-Plex Pd Barcoding kit [Standard Biotools]. All the samples were pooled after barcoding, followed by Fc and eosinophil blocking using FcX block and Heparin salt. Cell staining was carried out using a panel consisting of 40 antibodies for both surface and intracellular markers (Supplementary Table S2). After staining, cells were fixed and treated with iridium containing intercalator solution (Cell ID Intercalator Ir [Standard Biotools] and incubated overnight at 4 °C. The next day, cells were washed and resuspended in Maxpar water containing 10 % EQ4 four element calibration beads and the events acquired on Helios mass cytometer [Standard Biotools].

2.9. Analyses of CyTOF data

2.9.1. Data pre-processing

Raw FCS files were used for data pre-processing. To account for variability in instrument performance over time, the signals were first normalized using EQ4 calibration beads, which contain four elemental standards (Finck et al., 2013). Subsequently, the normalized files underwent quality control using the PeacoQC algorithm, which adeptly detects and filter out spurious and erroneous events (Emmaneel et al., 2022). To further improve data integrity, we assessed the quality of each FCS files based on its Average Overlap Frequency (AOF) scores. Files with AOF scores exceeding three standard deviations above the mean of all runs were excluded from downstream analysis (Amir et al., 2018). The filtered files were then de-barcoded to segregate multiplexed events into respective samples. Automated gating was applied on the Event Length and the Gaussian parameters (Center, Offset, Residual, and Width) using CyTOFClean package. Following cleaning, live single cells were identified and gated using automated algorithms from the flowDensity package using Ir (DNA) and cisplatin channels.

2.9.2. Unsupervised analysis

Due to the high variability in signal intensities between experimental runs, batch normalization was deemed ineffective. To minimize noise and facilitate unsupervised analysis, the marker intensities within each file were categorized into either three levels (low = 0, medium = 0.5, high = 1) or two levels (low = 0 and high = 1). Automated gaussian gating was performed with manual supervision, ensuring consistency in gate boundaries within each run, and uniformity within each donor across runs. The categorized expression levels were used for the unsupervised clustering as described in Supplementary data. Cells were first classified into three main cell populations: T cells: defined as CD3-positive and negative for lineage specific markers of other major cell populations (CD66b, CD19, CD56). Specifically, T cells were characterized as CD3 = 1, CD19 = 0, CD56 < 1, CD66b = 0, and positive for at least one of CD4, CD8 or TCRgd (CD4 = 1 or CD8 > 0 or TCRgd = 1); B cells: identified as CD19-positive and negative for CD66b, CD3, and CD56 (CD19 = 1, CD3 = 0, CD56 < 1, CD66b = 0), with HLA-DR expression greater than zero (HLA-DR > 0) and "Other" cells: defined as cells that did not fall into the T or B cell categories.

Each of the three major cell populations were clustered into a predefined number of clusters; T cells: 10, 20, 30, 40, 50 and 60 clusters; B cells: 5, 10, 20, 30, 40 clusters; and other cells: 5, 10, 20, 30, 40 clusters. To ensure non-redundancy in statistical analyses, only unique clusters were analysed further. First all clusters from the smallest predefined number of clusters were defined as unique clusters, then a cluster was retained as a new unique cluster if it contained less than 95 % of the cells from any previously defined unique cluster. Subsequent analysis of clusters was conducted separately for stimulated and unstimulated samples. Clusters where all samples for a given stimulation contained less than 0.1 % of total cells were excluded from further analysis.

The proportion of cells in each unique cluster for each sample were compared between treatments using a paired Wilcoxon test, treating each donor as its own control. A significance level of $p < 0.05$ was used to identify differentially expressed clusters. To account for variability on sampling, all analyses were repeated using four randomly drawn subsamples of 20000 cells. Only the cell clusters that were identified as significantly different in at least two of the four subsamples, in one or more of the treatment groups, were reported. These significant clusters were subjected to supervised gating assessment for validation as described below.

2.9.3. Manual gating procedure

Manual gating was done to support findings from the unsupervised analysis using the Cytobank platform (Beckman Coulter). For the manual procedure, live, $CD45^{+}$ singlet cells obtained after the data preprocessing were used. The gating hierarchy used to identify major

cell populations is provided in the Supplementary section Fig. S3 for the unstimulated samples and in Fig. S3 for the samples with combined exposure to Minusil particles with immune stimulants. These immune cell populations were further gated according to the major markers characterizing the cell populations of interest in the unsupervised clustering. Paired Wilcoxon test was used to verify the significance of the manual gated clusters.

3. Results

3.1. Cell viability and cytokine release in response to particle exposure

The viability data confirmed that Minusil particles were markedly more toxic than gQ particles to macrophages (Supplementary Fig. S2). Cellular viability was measured by the Alamar Blue assay and showed an approximate 50 % reduction in cellular metabolic activity in the Minusil treated cells and no reduction by gQ. Moreover, membrane integrity was significantly reduced by Minusil (2.9-fold increase) and more moderately by gQ (1.7-fold increase) treatments as measured by fold increase in LDH leakage compared to controls.

The concentration of eighteen cytokines in the macrophage CM was subsequently measured by multiplex analysis. The anti-inflammatory cytokine TGFβ as well as IL-13, IL-17a and MPO were excluded due to low detection frequencies. Of the fifteen remaining markers, all but IFNγ were significantly increased in the Minusil treated samples compared to the controls (Fig. 2; Supplementary Table S3). Most of these cytokines are involved in the initiation of pro-inflammatory responses. Several cytokines were augmented also in the gQ exposed samples, and the increases in CCL4, IL-1β, TNFα and CXCL8 reached significance. All fourteen cytokines, except for IFNα, were significantly higher in culture medium from the Minusil treated samples compared to the gQ samples (Supplementary Table S3).

3.2. Soluble cytokines in whole blood exposed to macrophage CM

The first set of experiments was performed with exposure of whole blood to CM from particle exposed THP-1 derived macrophage-like cells. Soluble cytokines were measured after 24- and 48-h exposure to CM. Data for fourteen of the eighteen cytokines are presented (Supplementary Table S3), while IL-13, IL-17a, IFNγ and IFNα are not presented due to low detection frequencies. Of the fourteen cytokines, seven (IL-1β, IL-6, IL-18, IL-23, CCL2, CCL3, CXCL10) were significantly upregulated by Minusil at the 24-h time point of which two (CCL2 and IL-6) did not reach significance in the adjusted analysis. TGFβ was significantly reduced in Minusil group compared to control in the unadjusted analysis. IL-1β, IL-6, IL-18, IL-23, CXCL10 were still significantly increased in the Minusil group at the 48-h timepoint, in addition to GM-CSF, but only the differences in IL-6, CXCL10 and IL-18 reached significance in the adjusted analysis. None of the cytokines were significantly different between the controls and the gQ exposed samples, whereas IL-18 levels were significantly higher in the Minusil compared to the gQ treated samples at both timepoints. Individual donor responses are shown in Fig. 3 for the cytokines that were significantly different in the Minusil compared to the control group at either 24 or 48 h (adjusted $p < 0.1$). For some of the cytokines (e.g. IL-18, CCL3) the majority of the donors showed increased levels in Minusil compared to control groups whereas for others (e.g. IL-6, CXCL10) the differences seem to be driven by a strong effect in a subgroup of the donors. Sex differences did not appear to explain the donor variability observed, but the potential effect of sex differences was not statistically tested due to the relatively low number of donors. Male and female donor identity is indicated in the graphs.

3.3. Differentially expressed cell clusters in whole blood after exposure to CM

To further characterise effects of exposure of whole blood to CM from particle exposed macrophages, we assessed changes in immune cell phenotypes by single cell mass cytometry using an antibody panel consisting of 40 surface and internal markers (Supplementary Table S2). Differentially expressed cell populations were identified by unsupervised clustering and subsequently confirmed by manual gating procedures (manual gating hierarchy in Supplementary Fig. S3). The frequencies of main cell populations for the different treatments are shown in Supplementary Fig. S5. No differences in frequencies of the main immune cell populations between exposures were observed. The data reveal a low percentage of neutrophiles compared to the composition of fresh whole blood, reflecting a gradual loss of neutrophiles during the 48-h culture period. Unsupervised clustering identified nine main cell populations as differentially expressed compared to control when clusters with less than 0.1 % of total cells were excluded. Eight of the nine clusters were confirmed to be differentially expressed in one or more treatment groups by manual gating and are summarized in Table 1 with the defining phenotypic markers given for each cluster. Expression

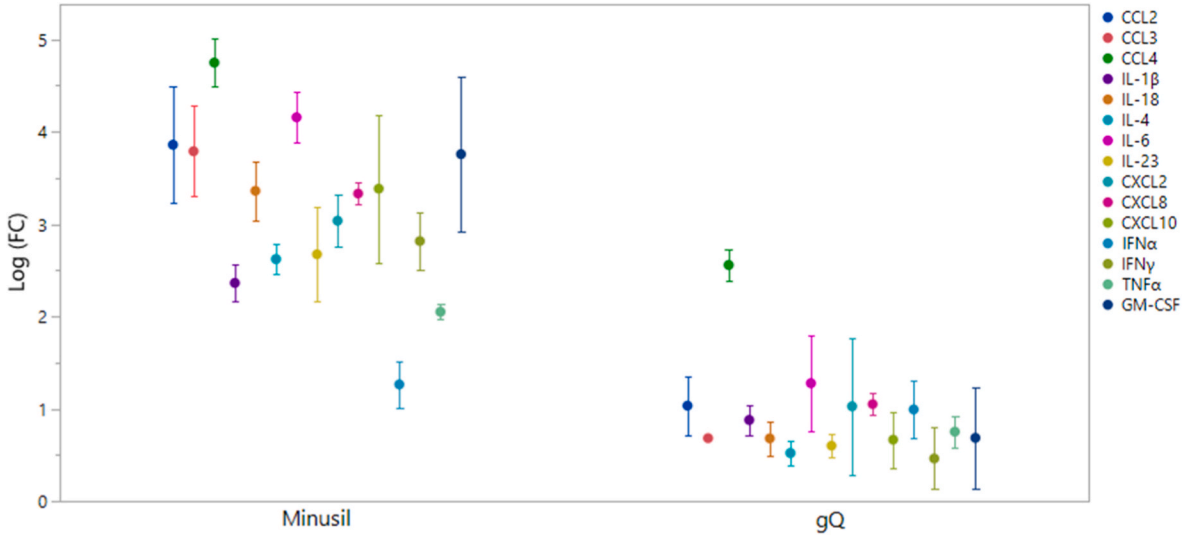

Fig. 2. Log Fold Change (FC) in cytokine concentrations in culture medium from particle-treated macrophages versus controls. Macrophages were exposed for 24 h to Minusil and gQ particles and concentrations of cytokines in the culture medium were measured. Mean log FC changes between control and particle exposed samples are shown, error bars = standard error.

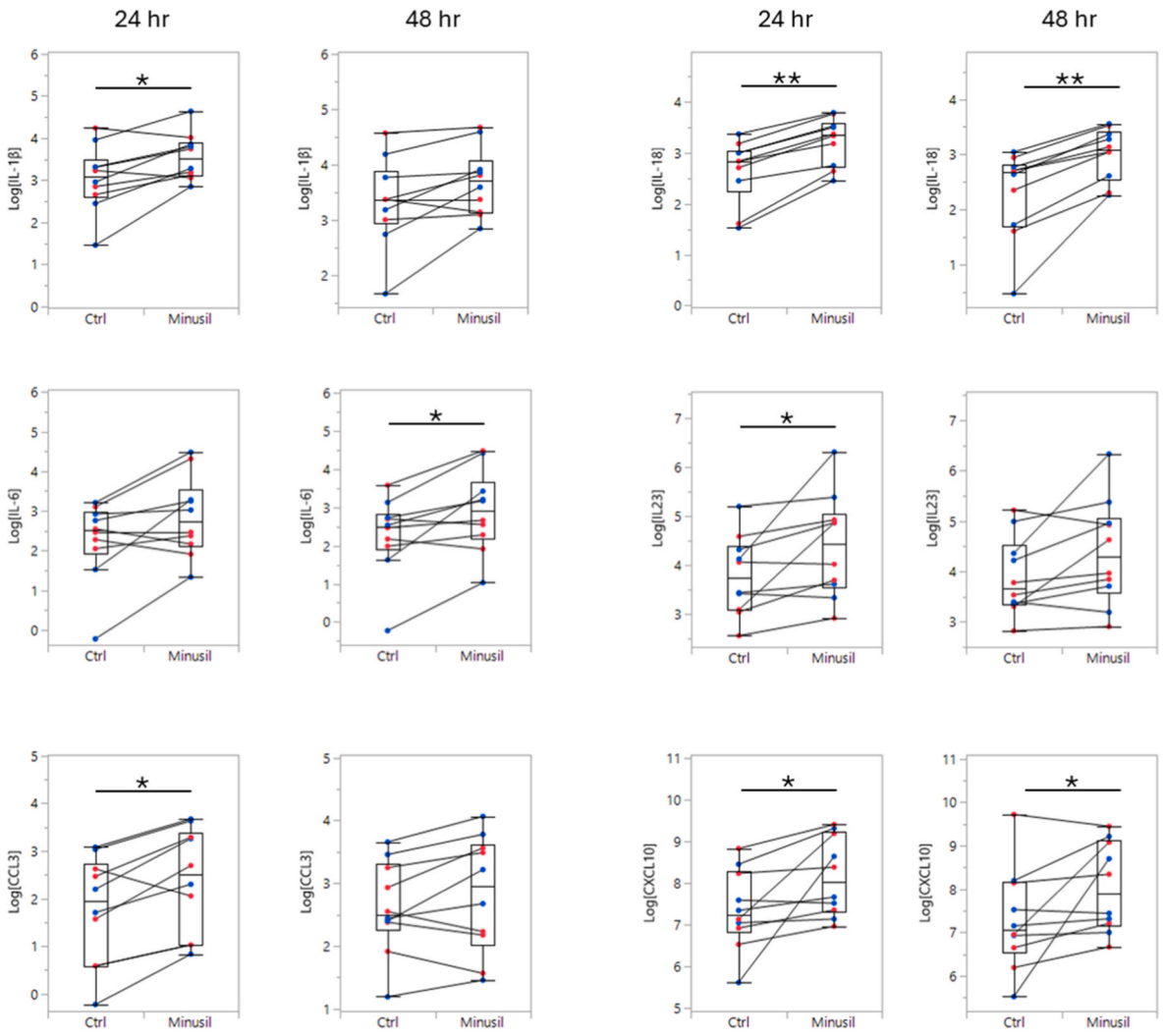

Fig. 3. Cytokine concentrations in whole blood. Log-transformed cytokine mean fluorescence level (MFI) levels in whole blood after incubation with macrophage control and Minusil-conditioned medium for 24 or 48 h are shown for IL-1β, IL-18, IL-6, IL-23, CCL3 and CXCL10. Boxes show median, 25 and 75 percentiles. Connected dots represent individual donor levels. Red: females, Blue: males, n = 10. *adj. $p < 0.1$, **adj. $p < 0.001$, compared to control. (For interpretation of the references to colour in this figure legend, the reader is referred to the Web version of this article.)

of all markers for each cluster are displayed in the marker plot in Supplementary Fig. S6.

Direct exposure of blood cells to IL-1β was included as a positive control for effects of inflammasome activation on immune cells. Five lymphocyte clusters and two monocyte/dendritic cell clusters were differentially expressed in the IL-1β exposed samples compared to controls (Table 1, Fig. 4).

All the B and T lymphocyte clusters (clusters 1–5) were significantly more frequent in the IL-1β treated cells compared to controls (Fig. 4). For clusters 1 and 2, $CD38^{hi}$ B and CD4 T cell subsets, respectively, a similar tendency was seen for the Minusil and gQ particle groups, but the differences did not reach significance or were not significant by both unsupervised and manual gating procedures (Table 1). The NK cell cluster (Cluster 6: $CD38^{hi}$, $CD56^{dim}$) was significantly increased in the Minusil treated cells compared to controls (Fig. 4), whereas two T-cell populations, cluster 3 ($IL\text{-}10^{+}$ naïve $CD4^{+}$ T cells) and cluster 4 ($CD161^{+}$ effector memory $CD8^{+}$ T cells) as well as a NKT cell population (cluster 5: $CD161^{+}$ NK-like T cells) were significantly differentially expressed in the IL-1β group only (Table 1, Fig. 4).

Among the myeloid cells, significantly decreased frequencies in the Minusil and IL-1β samples were seen for two clusters (clusters 7 and 8, Table 1 and Fig. 4). Cluster 7 resembles intermediate monocytes ($CD14^{+}$ and $CD16^{+}$) with expression of CD38 and several cytokines. A more modest, non-significant decrease in cluster 7 monocytes was seen for the gQ treated group.

Cluster 8 appeared to be a mix of non-classical monocytes and conventional dendritic cells ($HLA\text{-}DR^{+}$, $CD11c^{+}$, $CD14^{lo}$, $CD16^{lo\ +\ hi}$, $CD123^{-}$, $CD1c^{+/-}$). Further specification of dendritic cell clusters was thus done by manual gating. Manual gated conventional dendritic cells (cDCs: $HLA\text{-}DR^{+}$ $CD11c^{+}$ $CD14^{-}$) showed reduced frequencies in the Minusil and IL-1β groups (Fig. 4). A significant difference between the Minusil and the gQ groups was observed for cDC2 cells ($CD1c^{+}$) frequencies.

Interestingly, three of the lymphocyte clusters (1, 2 and 6) as well as the monocyte cluster (cluster 7) were characterised by a high expression of the early activation marker CD38.

3.4. *Effects of Minusil CM on whole blood responses to immune stimulation*

Circulating immune cells are mostly naïve or resting, so in a second set of experiments, an immune challenge was added to assess effects of Minusil CM on peripheral immune cell responses. gQ particles were not included in these experiments due to their lower potency in the first set

Table 1
Differentially expressed immune cell clusters identified following exposure to macrophage conditioned medium (CM). Whole blood was exposed to CM (Control, Minusil or gQ) or to the reference control IL-1β for 48 h. Cell clusters that were differentially expressed compared to control were identified by unsupervised analysis and confirmed by manual gating. Only clusters confirmed by manual gating for one or more conditions are shown. Main markers used for defining the differentially expressed clusters are listed.

Cluster number Annotation	Defining cluster markers	Minusil	gQ	IL-1β
1 CD38^{hi} Naïve/DN B cells	CD66b$^-$, CD3$^-$, CD19$^+$, CD27^{lo}, IgD$^{lo\text{-}hi}$, CCR7$^{lo\text{-}hi}$, CD38^{hi}, CXCR5$^+$, HLA-DR$^+$, CD45RA$^+$, CD69$^{lo\text{-}hi}$	↑*[a]	ns	↑*
2 CD38^{hi} CM/Naive CD4$^+$ T cells	CD66b$^-$, CD19$^-$, CD3$^+$, CD4$^+$, CCR7$^+$, CD45RA$^{lo\text{-}hi}$, CD27^{hi}, CD38^{hi}	↑*[a]	↑*[a]	↑*
3 IL-10$^+$ Naive CD4$^+$ T cells	CD66b$^-$, CD19$^-$, CD3$^+$, CD4$^+$, CCR7$^+$, CD45RA$^+$, CD27$^{lo\text{-}hi}$, IL-10$^+$	ns	ns	↑**
4 CD161$^+$ EM CD8$^+$ T cells	CD66b$^-$, CD19$^-$, CD3$^+$, CD8$^+$, CCR7$^{lo\text{-}me}$, CD45RA$^{lo\text{-}me}$, CD161$^+$, CD27$^{lo\text{-}hi}$, CD69$^+$, CCL4$^{lo\text{-}hi}$	ns	ns	↑**
5 CD161+ NKT cells	CD66b$^-$, CD19$^-$, CD3$^+$, CD56$^+$, CD8$^{lo\,+\,hi}$, CCR7$^{lo\text{-}me}$, CD45RA$^{lo\text{-}me}$, CD161$^{me\text{-}hi}$, CD69$^{lo\text{-}hi}$	ns	ns	↑*
6 CD38^{hi} CD56^{dim} NK cells	CD66b$^-$, CD19$^-$, CD3$^-$, CD56$^+$, CD16$^+$, CD161$^+$, CD38^{hi}	↑*	ns	ns
7 CD38^{hi} CD14$^+$ CD16$^+$ Intermediate Monocytes	CD66b$^-$, CD19$^-$, CD3$^-$, HLA-DR$^+$, CD11c$^+$, CD14$^+$, CD16$^+$, CD123$^-$, CD38^{hi}, IL21$^+$, CXCL8$^+$, CCL2$^+$, IFNα$^+$	↓*	ns	↓*
8 DC and Non-classical Monocytes	CD66b$^-$, CD19$^-$, CD3$^-$, HLA-DR$^+$, CD11c$^+$, CD16$^{lo\,+\,hi}$, CD14^{lo}, CD123$^-$	↓**	ns	↓*

↑ = significantly increased, and ↓ = significantly decreased cluster frequencies compared to the control group.
[a] significantly different in either unsupervised or manual gated population. Bold: significant both by unsupervised analysis and by manual gating. *$p < 0.05$; **$p < 0.005$, ns: non-significant.

of experiments. An immune stimulating cocktail was added to the samples during the final 4 h of the 48-h incubation with CM. In parallel samples, soluble cytokine levels (Fig. 5; Supplementary Table S3) and single cell profiling (Table 2) of whole blood phenotypes and intracellular cytokines were analysed.

3.4.1. *Soluble cytokines in stimulated whole blood exposed to Minusil CM*

As expected, many of the soluble cytokines were secreted at a higher level in the immune stimulated versus the unstimulated samples (Supplementary Table S3). In the immune stimulated samples, the concentrations of six cytokines were higher in the Minusil CM samples than in the control samples (IL-1β, GM-CSF, CCL2, IL-18, CXCL8, CXCL10), of which CCL2, IL-18 and CXCL8 remained significant in the adjusted analysis. All donors showed significantly higher concentrations in the Minusil CM exposed samples compared to the control samples after immune stimulation of these three cytokines that are primarily produced by myeloid cells (Fig. 5). The use of two different concentrations of immune stimulation cocktail did not affect the direction of change (Fig. 5).

3.4.2. *Differentially expressed cell clusters in stimulated whole blood cells exposed to Minusil CM*

The frequencies of main cell populations for Minusil CM and control exposures in the immune stimulated samples are shown in Supplementary Fig. S5. No differences between the Minusil CM and the control samples were observed. Unsupervised clustering defined seven distinct immune cell clusters as being differentially expressed between the control and Minusil CM treated samples, as detailed in Table 2. One B cell cluster, S1 (CD19$^+$, CD27^{lo}, IgD$^{lo\text{-}hi}$, HLA-DR$^+$, CXCR5$^+$, CD38^{hi}, CD69$^+$) and five clusters of CD3$^+$ T cells, namely S2 (CD4$^+$, CCR7$^{lo\text{-}hi}$, CD45RA$^{lo\text{-}hi}$, CD27$^+$, CD38^{hi}), S3 (CD4$^+$, CCR7$^+$, CD45RA$^+$, CD27$^+$, CD69$^+$, CD38^{hi}, CD25$^{lo\text{-}me}$, ICOS$^+$, IL-4$^{+)}$), S4 (CD8$^+$, CCR7$^{lo\text{-}me}$, CD45RA$^{lo\text{-}hi}$, CD27$^+$, CD161^{hi}, CD69$^+$), S5 (CD8$^+$, CCR7^{lo}, CD45RA$^{lo\text{-}hi}$, CD27$^{lo\text{-}me}$, CD69$^+$ CD57$^{lo\,+\,hi}$, CCL4$^+$ TNFα$^+$ and IFNγ$^+$ fraction), and S6 (CD8$^+$, CCR7$^+$, CD45RA$^+$, CD27$^+$, CD38^{hi}) were significantly elevated in the Minusil CM samples. Finally, a small mixed IdU$^+$ cell population (S7), was significantly reduced in the Minusil CM treated samples when compared to controls.

All the clusters identified as differentially expressed in the unsupervised analysis were corroborated by manual gating (see the manual gating hierarchy in Supplemental Fig. S3). The characterising phenotypic markers for each cluster are shown in Table 2. Expression of all markers for the seven clusters are shown in the marker plot (Supplementary Fig. S7).

As observed in the unstimulated samples, B and T lymphocyte clusters (clusters S1-S3 and S6) characterised by high expression of CD38 were differentially expressed (Fig. 6). The cells of the naïve/DN B-cell cluster also express the activation marker CD69 and the majority are positive for IL-4. Two CD38^{hi} CD4 T-cell clusters were identified (clusters 2 and 3). Cluster 3 represents naïve CD4$^+$ T cells expressing moderate to high levels of the T helper 2 (Th2) cell promoting cytokine IL-4, in addition to the activation markers CD38, ICOS and CD69. In addition, two CD8$^+$ EM T-cell clusters were increased. One of these clusters (S4) had a high expression of CD161 and CD69. Most of the cells were positive for CCL4 whereas a subpopulation also expressed TNFα. The high expression of CD161 suggests that this cluster may include CD8$^+$ MAIT cells. The other CD8$^+$ cluster (S5) consisted of CD161-negative polyfunctional cells, a majority of which were positive for CCL4, IFNγ and TNFα in addition to CD69 and ICOS (Fig. 6).

In addition, a small population of a mixed IdU$^+$ cell population (S7) were significantly reduced in the Minusil CM group when compared to controls (Table 2). Whether this population represents proliferating cells is somewhat uncertain as the cellular incorporation of IdU was modest.

Due to similarities of several of the differentially expressed CD38^{hi} lymphocyte subpopulations, a comparison between unstimulated and stimulated samples was performed. This comparison shows that the CD38^{hi} Naïve/DN B-cell and CD38^{hi} CD4$^+$ T-cell populations were significantly increased by Minusil CM in both stimulated and unstimulated samples (Supplementary Fig. S8). In addition, the CD38^{hi} CD56^{dim} NK population was found to be significantly increased in both conditions, whereas CD38^{hi} CD8$^+$ T-cell population was only induced in the Minusil CM samples in the immune-stimulated samples.

4. Discussion

Due to their low solubility, RCS cause persistent inflammation, a central factor in particle-induced lung and systemic disease (Poland et al., 2024). In a recent review (Leinardi et al., 2022), we describe potential consequences of silica-induced release of DAMPs from stressed and dying macrophages and propose mechanisms driving the progress of certain silica–related lung and autoimmune diseases. To bridge the effects of RCS exposure with the risk of systemic diseases, we have characterised downstream effects of CM from particle exposed THP-1 derived macrophage-like cells on blood cell phenotypes and their functional markers. We compared two types of α-quartz particles to elucidate the importance of particle surface characteristics as a pivotal factor for mediating downstream immunomodulatory responses.

The NFS-rich Minusil particles are shown to be markedly more toxic to macrophages compared to the synthetic NFS-poor gQ particles. This is evidenced by a stronger impairment of cell viability and a higher release of a range of cytokines and chemokines, including IL-1β, IL-4, IL-6, IL-18, TNFα, CCL2, CCL3, CXCL8 and CXCL10. Several studies have

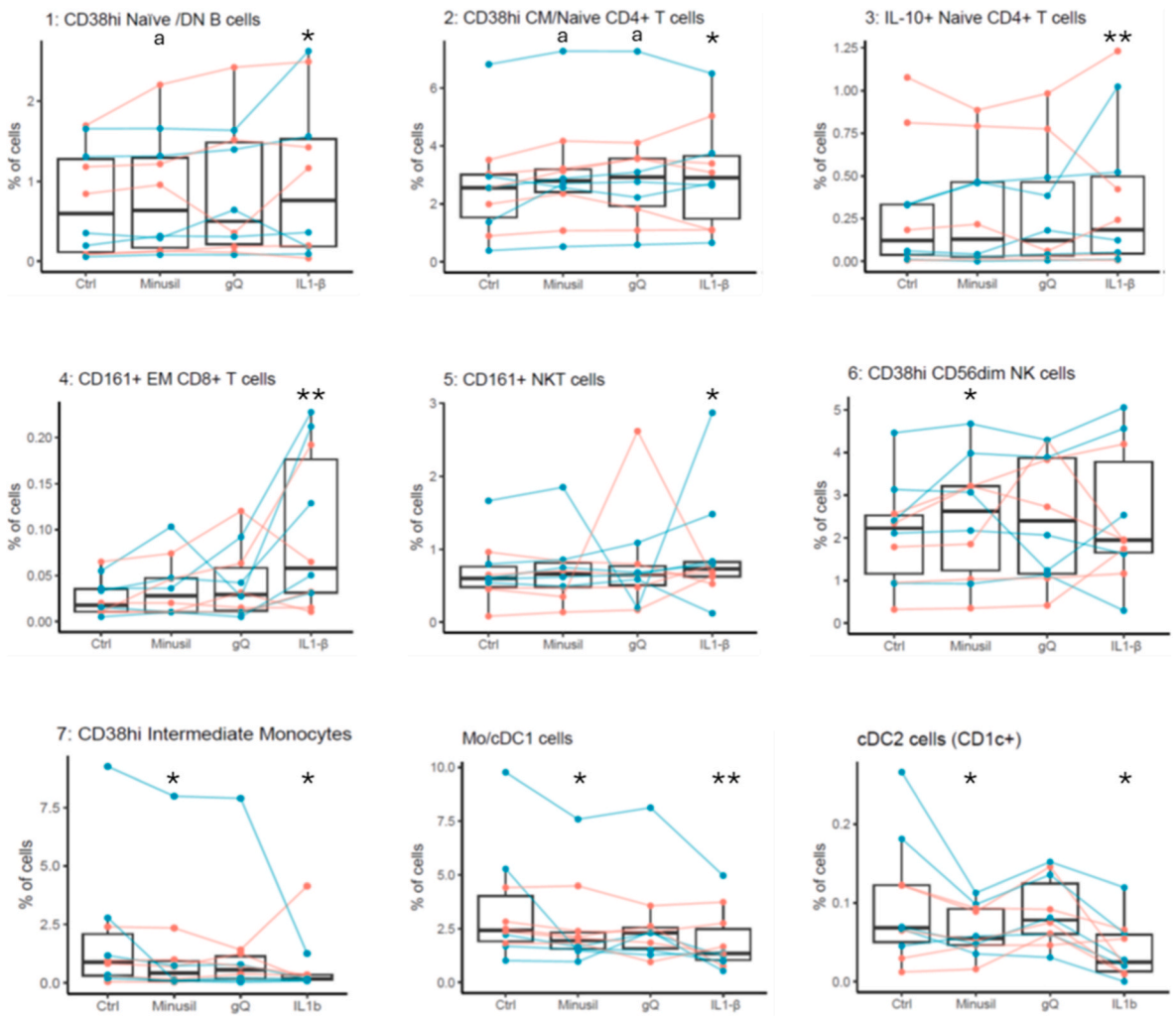

Fig. 4. Frequencies of differentially expressed immune cell clusters. Comparison of cell frequencies between whole blood samples treated with CM from control, Minusil, gQ, and IL-1β samples. In the two upper panels, lymphocyte subpopulations are shown: B-cell (cluster 1; $CD27^{lo}$, $CD38^{hi}$, $CXCR5^{+}$, $HLA\text{-}DR^{+}$, $CD45RA^{+}$), T-cell (clusters 2–5) and NK cell (cluster 6; $CD56^{dim}$, $CD16^{+}$, $CD161^{+}$, $CD38^{hi}$) clusters. In the lower panel, monocyte and dendritic cell subpopulations are shown: intermediate monocytes (cluster 7), non-classical monocytes and conventional dendritic cells (Mo/cDC1) and conventional $CD1c^{+}$ dendritic cells (cDC2). The DC populations were manually gated. Connected dots represent individual donor frequencies. Red: females, Blue: males. [a] significant compared to control by either unsupervised or manual gating. *$p < 0.05$ and **$p < 0.005$, significant compared to control in both unsupervised and manual gated subpopulations. (For interpretation of the references to colour in this figure legend, the reader is referred to the Web version of this article.)

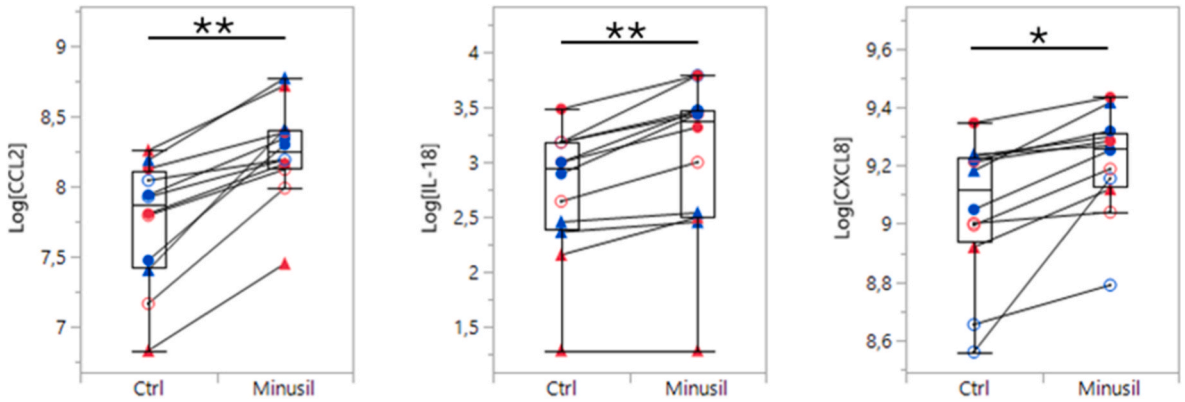

Fig. 5. Concentration of soluble chemokines in blood in immune stimulated samples. Log-transformed cytokine MFI levels [in whole blood after 48-hr incubation with macrophage control and Minusil CM, and 4-h immune stimulation are shown. Boxes show median, 25 and 75 percentiles. Connected dots represent individual donor levels, n = 12. Filled symbols: low immune stimulant concentration, triangles for experiment 1 and circles for experiment 2; Open circles: high immunostimulant concentration (experiment 3). Red: females, Blue: Males. Significant differences compared to control are indicated by * adjusted $p < 0.1$, **adjusted $p < 0.01$. (For interpretation of the references to colour in this figure legend, the reader is referred to the Web version of this article.)

Table 2
Differentially expressed cell clusters in immune stimulated blood cell after macrophage conditioned medium (CM). Whole blood was exposed for 48 h to CM from control or Minusil treated macrophages with an immune stimulation during the last 4 h. Differentially expressed cell clusters were identified by unsupervised analysis and confirmed by manual gating. Only clusters confirmed by manual gating are shown. Main markers used for defining the differentially expressed clusters are listed.

Cluster number Annotation	Defining cluster markers	Minusil vs Ctrl
S1 $CD38^{hi}$ Naïve/DN B cells	$CD66b^{-}$, $CD3^{-}$, $CD19^{+}$, $CD27^{lo}$, $IgD^{lo\text{-}hi}$, $HLA\text{-}DR^{+}$, $CXCR5^{+}$, $CD38^{hi}$, $CD69^{+}$	↑*
S2 $CD38^{hi}$ $CD4^{+}$ T cells	$CD66b^{-}$, $CD19^{-}$, $CD3^{+}$, $CD4^{+}$, $CCR7^{lo\text{-}hi}$, $CD45RA^{lo\text{-}hi}$, $CD27^{+}$, $CD38^{hi}$	↑**
S3 $CD38^{hi}$ Naïve $CD4^{+}$ T cells	$CD66b^{-}$, $CD19^{-}$, $CD3^{+}$, $CD4^{+}$, $CCR7^{+}$, $CD45RA^{+}$, $CD27^{+}$, $CD69^{+}$, $CD38^{hi}$, $CD25^{lo\text{-}me}$, $ICOS^{+}$, $IL\text{-}4^{+}$	↑**
S4 $CD161^{hi}$ EM $CD8^{+}$ T cells	$CD66b^{-}$, $CD19^{-}$, $CD3^{+}$, CD8, $CCR7^{lo\text{-}me}$, $CD45RA^{lo\text{-}hi}$, $CD27^{+}$, $CD161^{hi}$, $CD69^{+}$	↑**
S5 EM $CD8^{+}$ T cells, polyfunctional	$CD66b^{-}$, $CD19^{-}$, $CD3^{+}$, $CD8^{+}$, $CCR7^{lo}$, $CD45RA^{lo\text{-}hi}$, $CD27^{lo\text{-}me}$, $CD69^{+}$, $CD57^{lo\ +\ hi}$, $CCL4^{+}$, $TNF\alpha^{+}$, $IFN\gamma^{lo\text{-}hi}$	↑**
S6 $CD38^{hi}$ Naïve $CD8^{+}$ T cells	$CD66b^{-}$, $CD19^{-}$, $CD3^{+}$, $CD8^{+}$, $CCR7^{+}$, $CD45RA^{+}$, $CD27^{+}$, $CD38^{hi}$	↑**
S7 IdU^{+} cells	IdU^{+}	↓**

↑ = increased and ↓ = decreased cluster frequency compared to the control group. *$p < 0.05$; **$p < 0.005$.

implicated the chemokines CCL2, CCL3, CXCL8 and CXCL10, as central for immune cell recruitment and activation as well as being associated with disease severity (Keane, 2008; Giordano et al., 2010; Ha et al., 2017; Lee et al., 2017; Yang et al., 2023). Our findings aligne with previous reports indicating that Minusil exposure causes macrophage damage, NLRP3 inflammasome activation and subsequent release of pro-inflammatory markers (Cassel et al., 2008; Hornung et al., 2008; Leinardi et al., 2020), along with our own data showing that Minusil is far more potent than the gQ particles (Pavan et al., 2020, 2024; Leinardi et al., 2023).

Subsequent exposure of whole blood to CM from macrophages-like cells exposed to Minusil resulted in significant increased levels of the cytokines IL-1β, IL-6, IL-18, IL-23, CCL3 and CXCL10 relative to controls, following 24 and/or 48 h of exposure. In contrast, cells exposed to gQ CM showed no significant changes in cytokine levels. The highest fold change was observed in CXCL10, whereas the most statistically significant difference observed was a sustained increase of IL-18 across all donors with Minusil CM treated whole blood cells compared to controls. Increased concentrations of CXCL10 have been previously reported in sputum of patients with silicosis (Benmerzoug et al., 2018). The NLR family pyrin domain containing 3 (NLRP3) inflammasome and IL-1β has been implicated in silica induced silicosis in animal models (Srivastava et al., 2002; Cassel et al., 2008; Guo et al., 2013). Notably, elevated plasma levels of the NLRP3 inflammasome associated marker IL-18 has been reported in silicosis patients as well as in patients with autoimmune diseases.

(Nadif et al., 2006; She et al., 2021; Ihim et al., 2022; Campos-Caro et al., 2023; Liu et al., 2024). Moreover, following a 4-h immune stimulation, an increase was detected in CCL2 and CXCL8, along with IL-18, in whole blood exposed to Minusil CM. Increased levels of CCL2 has been linked to pulmonary inflammation and fibrosis in rodents (Saarimäki et al., 2025). The cytokines profile induced in Minusil CM exposed blood cells mirrors those reported in patients with simple silicosis (Campos-Caro et al., 2023).

The current literature provides limited information on the phenotypic changes in peripheral immune cell following exposure to micro-

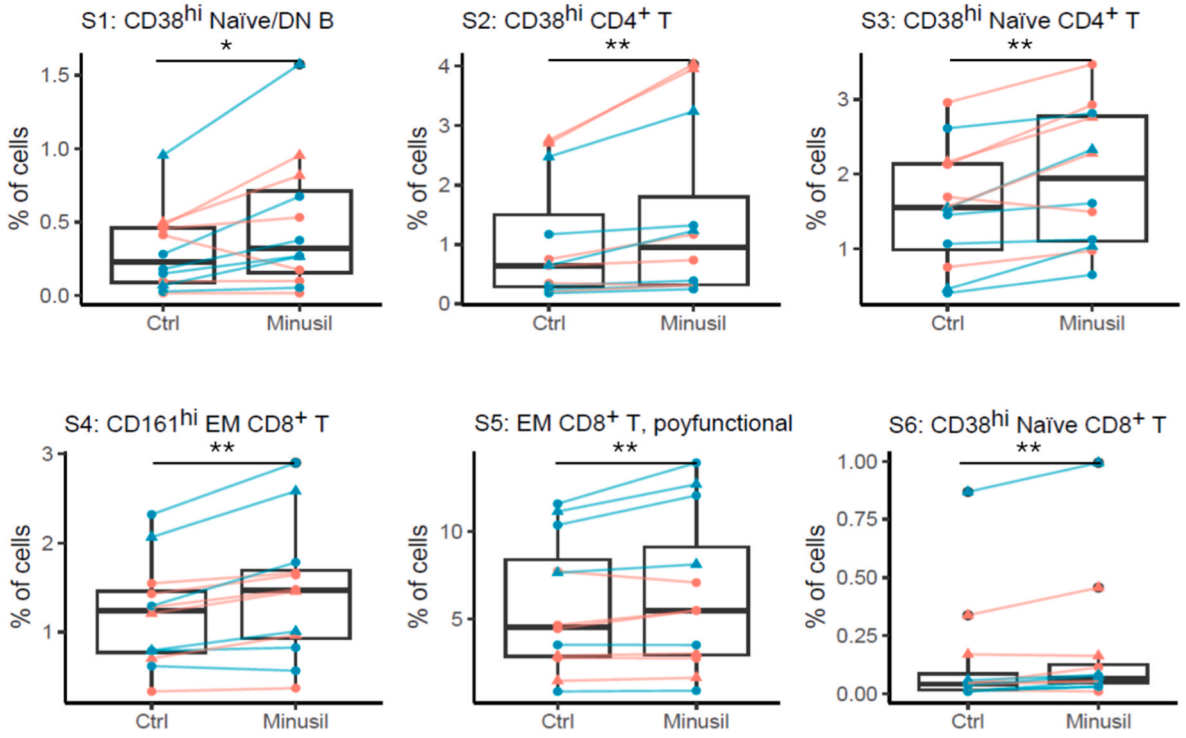

Fig. 6. Frequencies of differentially expressed cell clusters in whole blood cells exposed to Minusil and control CM followed by a 4-h immune stimulation. Comparison of cell frequencies of the lymphocyte clusters S1-S6 differing between the control and Minusil CM treated cells. S1, S2, S3 and S6 expressing high levels of CD38, S4 expressing high levels of CD161 and S5 being polyfunctional cells. Connected dots represent individual donor frequencies. Circles indicate samples with low concentrations of immune stimulation cocktail, and triangles indicate samples with high concentrations. Red: females, Blue: males. Significant differences are indicated by * $p < 0.05$, **$p < 0.005$. (For interpretation of the references to colour in this figure legend, the reader is referred to the Web version of this article.)

sized crystalline silica. To characterise the immunomodulatory effects of indirect particle exposure at the single cell level, we employed mass cytometry (CyTOF) with a panel of 40 antibodies. This allowed for the simultaneous detection of major cell phenotype and functional markers, including surface activation proteins, intracellular cytokines, chemokines and proliferation markers. In the cells not exposed to an immune stimulation cocktail, the most significant effects of particle treatment were observed in innate cells subpopulations. Following a 48 h culture period, the frequency of classical monocytes ($CD14^{+}$, $CD16^{-}$) in whole blood was generally low compared to nonclassical and intermediate monocyte populations, irrespective of treatment. A similar decline in classical monocytes during culture has been previously reported (Tran et al., 2019) and may be attributed to changes in CD14 and CD16 surface markers during extended culture. Whole blood treated with Minusil CM showed a reduction in intermediate-like monocytes (Cluster 7), whereas the gQ CM treated cells showed a lesser, non-significant, reduction. Manual gating of dendritic cell populations revealed reduced frequencies of conventional dendritic cells (cDC1 and cDC2) in the Minusil CM treated cells as compared to controls. In contrast, these dendritic cell populations were not reduced in the gQ CM treated cells. Consistent with the presence of more immature dendritic cells, indirect exposure to silica particles has been shown to down-regulate dendritic cells maturation markers including HLA-DR and CD80, thereby suppressing dendritic cell activity (Liu et al., 2019). Nevertheless, we cannot exclude the possibility that the observed reductions in monocyte and dendritic cell subpopulations may be caused by reduced cell survival and/or by cell loss due to e.g. increased adherence to the sides of the incubation tubes. It is known that activated monocytes and immature dendritic cells have a propensity to adhere to plastic surfaces (Delirezh et al., 2013).

IL-1β is recognised as a critical mediator of lung inflammation and fibrosis induced by crystalline silica exposure (Srivastava et al., 2002; Guo et al., 2013; Weng et al., 2015). In this study, IL-1β was added directly into whole blood samples as a positive control to facilitate the interpretation of the single cell data. Of note, the IL-1β concentration added to the blood cells (25 ng/ml) was much higher than the concentrations measured in the whole blood samples in the present study following exposure to Minusil CM and higher than the levels reported in plasma from patients with silicosis, autoinflammatory and autoimmune diseases that are generally in the lower pg/ml range (Dinarello, 2011; Mende et al., 2018). Regarding adaptive cell, IL-1β significantly increased frequencies of several $CD38^{hi}$ B and T lymphocyte populations. Increases in $CD38^{hi}$ lymphocyte populations were also suggested for the particle exposed whole blood, although only the increase in the $CD38^{hi}$ $CD56^{dim}$ NK population reached statistical significance across both unsupervised and manual gating procedures. Importantly, a similar increase in $CD38^{hi}$ lymphocyte populations were observed in the Minusil CM exposed cells following the addition of an immune stimulation cocktail.

CD38 can function both as a receptor and as a central NAD^{+}-consuming enzyme (Zeidler et al., 2022; Ghosh et al., 2023). Its upregulation is regarded as an early sign of immune cell activation and has been shown to play a critical role in inflammatory and autoimmune diseases (Pavón et al., 2013; Piedra-Quintero et al., 2020). Moreover, CD38 is known to modulate both the number and function of T cells (Li et al., 2022). Increased frequencies of CD38-positive CD4 T cells were reported in blood and in bronchoalveolar lavage fluid (BALF) of patients with newly diagnosed pulmonary sarcoidosis (Aleksonienė et al., 2021). Our findings thus suggest that RCS exposure, as well as IL-1β activity, induce early activation of naïve lymphocytes. To our knowledge, changes in CD38-positive lymphocytes due to occupational RCS exposure or in individuals with silicosis have not been previously reported.

Additionally, in blood cells treated with the immune stimulation cocktail, two effector memory (EM) cytotoxic T-cell populations ($CD8^{+}$; Clusters S4 and S5) were identified as more frequent in the Minusil CM treated cells compared to controls. These two populations differed in the absence or presence of the C-type lectin-like receptor CD161. CD161 is expressed on subsets of T-cells including $CD8^{+}$ T-cells and may have both a co-stimulatory and a co-inhibitory function (Ussher et al., 2014; Konduri et al., 2021). Cluster S4 may include innate-like mucosal-associated invariant T (MAIT) cells as these represent the majority of the $CD161^{hi}$ $CD8^{+}$ T cell population in blood (Fergusson et al., 2014). MAIT cells have been proposed to play a role in the development and progression of autoimmune diseases (Fan et al., 2023). Unfortunately, our antibody panel did not include the typical marker TCR Vα7.2+ needed to properly identify MAIT cells. Manual gating of $CD8^{+}$, $CD161^{-}$ EM T-cell population (cluster S5) showed that the frequency of the subpopulation positive for CD57 was increased in the Minusil CM treated cells. These cells were polyfunctional as they expressed high levels of the proinflammatory markers CCL4, IFNγ and TNFα. Previous studies report that $CD8^{+}$ T cells expressing CD57 are characterized by increased levels of pro-inflammatory and cytolytic molecules and have been implicated in inflammatory conditions, including in autoimmune disease (Strioga et al., 2011; Huang et al., 2020; Abbas and Akbar, 2021).

Barcoding was used to reduce technical variability between donors of the same experiment. Additional sources of variability in the present study include the use of different donors and differences in the conditioned medium as it was prepared fresh for each experiment. A limitation of the current study is that we used a high concentration of particles not representative of occupational exposure concentrations. However, particle dose should reflect the dose of inhaled particles that is accumulated on the alveolar surface over time. Due to the persistence of the particles in the lung, RCS has been shown to creating a prolonged pro-inflammatory signal (Leung et al., 2012). For this study, we wanted to achieve a certain level of cell death to be able to study effects of CM from stressed and dying macrophage-like cells on peripheral immune cells as this is hypothesised to be important for systemic silica-induced disease. Moreover, we only model the initial responses to RCS exposure and not inflammation resolution or delayed pathogenic responses and tissue interactions. The tissue resident macrophages are reported to have lower immunoreactivity than monocyte derived macrophages recruited to the lungs upon injury (Kulikauskaite and Wack, 2020). THP-1 is a monocytic leukemia cell line and THP-1 derived macrophages are thus likely a better model for studies of the responses of the recruited than the resident lung macrophages. THP-1 derived macrophage-like cells have a proficient NLRP3 inflammasome response (Zhou et al., 2011) and has proved to be useful in studies of crystalline silica particle toxicity (Chanput et al., 2014; Ruijter et al., 2025). A novelty of the present study is the detailed profiling of immune cell changes in phenotypic and functional markers in response to Minusil CM. In addition, particle-induced changes in immune cell function were assessed by challenging the cells with an immune stimulation cocktail. The stimulation cocktail, albeit non-physiological, includes a combination of viral, bacterial and more general immune stimulus. It was used to induce an activation response of a broad set of immune cell types, since resting blood immune cells needs stimuli to evaluate their functional states. The comparison of two similar α-quartz particles differing in the presence of reactive NFS-groups and in the proinflammatory and disease promoting activities (Pavan et al., 2020, 2024) provides further insight on the cellular changes that may be related to disease development.

In summary, exposure to Minusil particles induced a marked pro-inflammatory response in exposed THP-1 derived macrophage like cells, contrasting with the response to synthetic NFS-poor gQ particles. Whole blood exposed to CM from Minusil-treated cells for 24 and 48 h showed significantly elevated levels of soluble pro-inflammatory cytokines and chemokines. These increases ranged between 1.4 and 2.1-fold for IL-1β, IL-18, IL-6, IL-23, and CCL3, and a 5.5-fold increase for CXCL10. In contrast, whole blood exposed to CM from gQ-treated cells did not show significant changes in cytokine levels, underscoring the low inflammogenic potential of the synthetic particles.

At the single cell level, the main findings in whole blood exposed to Minusil CM compared to control were: i) altered monocyte and dendritic

cell subpopulation frequencies, ii) increased frequencies of NK, naïve B and naïve T lymphocyte subpopulations characterized by high expression of CD38, iii) following a 4-h immune stimulation, increased frequencies was observed of two effector memory $CD8^+$ T lymphocyte population, with one expressing high level of CD161 and the other being polyfunctional,.

By employing an *ex vivo* indirect exposure model, we provide novel data on potential links between RCS-induced macrophage toxicity and the modulation of innate and adaptive immune cells. Follow-up studies involving peripheral immune cells in occupational cohorts or animal models are essential to determine whether our *ex vivo* findings are applicable to *in vivo* contexts.

CRediT authorship contribution statement

Evangel Kummari: Writing – review & editing, Writing – original draft, Methodology. **Anja Bråthen Kristoffersen:** Writing – review & editing, Writing – original draft, Formal analysis, Data curation. **Sabin Bhandari:** Writing – review & editing, Writing – original draft, Formal analysis, Data curation. **Hege Hjertholm:** Writing – review & editing, Methodology. **Hubert Dirven:** Writing – review & editing, Project administration, Funding acquisition, Conceptualization. **Sarah E. Josefsson:** Writing – review & editing, Methodology. **François Huaux:** Writing – review & editing, Resources, Project administration, Funding acquisition, Conceptualization. **Riccardo Leinardi:** Writing – review & editing, Resources, Funding acquisition, Conceptualization. **Cristina Pavan:** Writing – review & editing, Writing – original draft, Resources. **Manosij Ghosh:** Writing – review & editing, Project administration, Funding acquisition, Conceptualization. **Peter Hoet:** Writing – review & editing, Project administration, Funding acquisition, Conceptualization. **Unni C. Nygaard:** Writing – review & editing, Writing – original draft, Conceptualization. **Birgitte Lindeman:** Writing – review & editing, Writing – original draft, Project administration, Methodology, Funding acquisition, Conceptualization.

Funding

The study has received funding from the European Union's Horizon 2020 research project Eximious (grant agreement No 874707). The authors would also like to acknowledge funding and support from colleagues at the Norwegian Institute of Public Health.

Declaration of competing interest

The authors declare that they have no known competing financial interests or personal relationships that could have appeared to influence the work reported in this paper.

Acknowledgement

The authors thank Tonje Skuland, Leni Ekeren and Jarle Ballangby for their help with Min-U-Sil 5 particles and THP-1 cells.

Appendix A. Supplementary data

Supplementary data to this article can be found online at https://doi.org/10.1016/j.envres.2025.123661.

Glossary

CM	Conditioned medium
CyTOF	Cytometry by time of flight
DAMPs	Damage-associated molecular patterns
DC	Dendritic cell
gQ	Synthetic as grown α-quartz particles
NK	Natural killer cell
Minusil	Min-U-Sil 5 α-quartz particles
MMAD	Mass median aerodynamic diameter
NFS	Nearly free silanols
RCS	Respirable crystalline silica

Data availability

Data will be made available on request.

References

Abbas, A.A., Akbar, A.N., 2021. Induction of T cell senescence by cytokine induced bystander activation. Frontiers in Aging 2. https://doi.org/10.3389/fragi.2021.714239.

Aleksonienė, R., Besusparis, J., Gruslys, V., Jurgauskienė, L., Laurinavičienė, A., Laurinavičius, A., Malickaitė, R., Norkūnienė, J., Zablockis, R., Žurauskas, E., Danila, E., 2021. CD31(+), CD38(+), CD44(+), and CD103(+) lymphocytes in peripheral blood, bronchoalveolar lavage fluid and lung biopsy tissue in sarcoid patients and controls. J. Thorac. Dis. 13, 2300–2318. https://doi.org/10.21037/jtd-20-2396.

Amir, E.D., Guo, X.V., Mayovska, O., Rahman, A.H., 2018. Average overlap frequency: a simple metric to evaluate staining quality and community identification in high dimensional mass cytometry experiments. J. Immunol. Methods 453, 20–29. https://doi.org/10.1016/j.jim.2017.08.011.

ATSDR, 2019. Toxicological Profile for Silica. Agency for Toxic Substances and Disease Registry (ATSDR, Atlanta, GA, 59198. https://doi.org/10.15620/cdc.

Barnes, H., Goh, N.S.L., Leong, T.L., Hoy, R., 2019. Silica-associated lung disease: an old-world exposure in modern industries. Respirology 24, 1165–1175. https://doi.org/10.1111/resp.13695.

Bellomo, C., Lagostina, V., Pavan, C., Paganini, M.C., Turci, F., 2024. Reaction with water vapor defines surface reconstruction and membranolytic activity of quartz milled in different molecular environments. Small 20, 2308369. https://doi.org/10.1002/smll.202308369.

Benmerzoug, S., Rose, S., Bounab, B., Gosset, D., Duneau, L., Chenuet, P., Mollet, L., Le Bert, M., Lambers, C., Geleff, S., et al., 2018. STING-dependent sensing of self-DNA drives silica-induced lung inflammation. Nat. Commun. 9, 5226. https://doi.org/10.1038/s41467-018-07425-1.

Brown, J.S., Gordon, T., Price, O., Asgharian, B., 2013. Thoracic and respirable particle definitions for human health risk assessment. Part. Fibre Toxicol. 10, 12. https://doi.org/10.1186/1743-8977-10-12.

Campos-Caro, A., Jiménez-Gómez, G., García-Núñez, A., Hidalgo-Molina, A., León-Jiménez, A., 2023. Plasma cytokine profiling reveals differences between silicotic patients with simple silicosis and those with progressive massive fibrosis caused by engineered stone. Int. J. Mol. Sci. 24. https://doi.org/10.3390/ijms24021541.

Cassel, S.L., Eisenbarth, S.C., Iyer, S.S., Sadler, J.J., Colegio, O.R., Tephly, L.A., Carter, A. B., Rothman, P.B., Flavell, R.A., Sutterwala, F.S., 2008. The Nalp3 inflammasome is essential for the development of silicosis. Proc. Natl. Acad. Sci. U. S. A. 105, 9035–9040. https://doi.org/10.1073/pnas.0803933105.

Castranova, V., 1994. Generation of oxygen radicals and mechanisms of injury prevention. Environ. Health Perspect. 102, 65–68. https://doi.org/10.1289/ehp.94102s1065.

Chanput, W., Mes, J.J., Wichers, H.J., 2014. THP-1 cell line: an in vitro cell model for immune modulation approach. Int. Immunopharmacol. 23, 37–45. https://doi.org/10.1016/j.intimp.2014.08.002.

Chen, S., Liu, M., Xie, F., 2022. Global and national burden and trends of mortality and disability-adjusted life years for silicosis, from 1990 to 2019: results from the global burden of disease study 2019. BMC Pulm. Med. 22, 240. https://doi.org/10.1186/s12890-022-02040-9.

Cullinan, P., Muñoz, X., Suojalehto, H., Agius, R., Jindal, S., Sigsgaard, T., Blomberg, A., Charpin, D., Annesi-Maesano, I., Gulati, M., et al., 2017. Occupational lung diseases: from old and novel exposures to effective preventive strategies. Lancet Respir. Med. 5, 445–455. https://doi.org/10.1016/s2213-2600(16)30424-6.

DECOS, 2024. Respirable Crystalline Silica. Evaluation of Health Hazards as Basis for an Occupational Exposure Limit. Health Council of the Netherlands: Dutch Expert Committee on Occupational Safety, The Hague. https://www.healthcouncil.nl/documents/advisory-reports/2024/09/10/respirable-crystalline-silica.

Delabre, L., Houot, M.T., Burtin, A., Pilorget, C., 2023. Occupational exposure to silica dust in France: an ongoing concern. Scand. J. Work. Environ. Health 49, 526–534. https://doi.org/10.5271/sjweh.4105.

Delirezh, N., Shojaeefar, E., Parvin, P., Asadi, B., 2013. Comparison the effects of two monocyte isolation methods, plastic adherence and magnetic activated cell sorting methods, on phagocytic activity of generated dendritic cells. Cell J 15, 218–223. PMID: 24027662; PMCID: PMC3769603.

Dinarello, C.A., 2011. Blocking interleukin-1β in acute and chronic autoinflammatory diseases. J. Intern. Med. 269, 16–28. https://doi.org/10.1111/j.1365-2796.2010.02313.x.

Donaldson, K., Borm, P.J.A., 1998. The quartz hazard: a variable entity. Ann. Occup. Hyg. 42, 287–294. https://doi.org/10.1093/annhyg/42.5.287.

Emmaneel, A., Quintelier, K., Sichien, D., Rybakowska, P., Marañón, C., Alarcón-Riquelme, M.E., Van Isterdael, G., Van Gassen, S., Saeys, Y., 2022. PeacoQC: Peak-based selection of high quality cytometry data. Cytometry A 101, 325–338. https://doi.org/10.1002/cyto.a.24501.

Fan, Q., Nan, H., Li, Z., Li, B., Zhang, F., Bi, L., 2023. New insights into MAIT cells in autoimmune diseases. Biomed. Pharmacother. 159, 114250. https://doi.org/10.1016/j.biopha.2023.114250.
Fazio, J.C., Viragh, K., Houlroyd, J., Gandhi, S.A., 2025. A review of silicosis and other silica-related diseases in the engineered stone countertop processing industry. J. Occup. Med. Toxicol. 20, 9. https://doi.org/10.1186/s12995-025-00455-8.
Fergusson, J.R., Smith, K.E., Fleming, V.M., Rajoriya, N., Newell, E.W., Simmons, R., Marchi, E., Björkander, S., Kang, Y.H., Swadling, L., et al., 2014. CD161 defines a transcriptional and functional phenotype across distinct human T cell lineages. Cell Rep. 9, 1075–1088. https://doi.org/10.1016/j.celrep.2014.09.045.
Finck, R., Simonds, E.F., Jager, A., Krishnaswamy, S., Sachs, K., Fantl, W., Pe'er, D., Nolan, G.P., Bendall, S.C., 2013. Normalization of mass cytometry data with bead standards. Cytometry A 83, 483–494. https://doi.org/10.1002/cyto.a.22271.
Fireman, E.M., Fireman Klein, E., 2024. Association between silicosis and autoimmune disease. Curr. Opin. Allergy Clin. Immunol. 24, 45–50. https://doi.org/10.1097/aci.0000000000000966.
Fireman, E., Mahamed, A.E., Rosengarten, D., Ophir, N.N., Kramer, M.R., 2021. Quantitation of silica contents in lung explants of transplanted patients: artificial stone-induced silicosis vs. idiopathic pulmonary fibrosis. Int. J. Environ. Res. Publ. Health 18. https://doi.org/10.3390/ijerph18147237.
Ghosh, A., Khanam, A., Ray, K., Mathur, P., Subramanian, A., Poonia, B., Kottilil, S., 2023. CD38: an ecto-enzyme with functional diversity in T cells. Front. Immunol. 14, 1146791. https://doi.org/10.3389/fimmu.2023.1146791.
Giordano, G., van den Brûle, S., Lo, Re S., Triqueneaux, P., Uwambayinema, F., Yakoub, Y., Couillin, I., Ryffel, B., Michiels, T., Renauld, J.C., et al., 2010. Type I interferon signaling contributes to chronic inflammation in a murine model of silicosis. Toxicol. Sci. 116, 682–692. https://doi.org/10.1093/toxsci/kfq158.
Gobindlal, K., Zujovic, Z., Yadav, P., Sperry, J., Weber, C.C., 2021. The mechanism of surface-radical generation and amorphization of crystalline quartz sand upon mechanochemical grinding. J. Phys. Chem. C 125, 20877–20886. https://doi.org/10.1021/acs.jpcc.1c06069.
Guo, J., Gu, N., Chen, J., Shi, T., Zhou, Y., Rong, Y., Zhou, T., Yang, W., Cui, X., Chen, W., 2013. Neutralization of interleukin-1 beta attenuates silica-induced lung inflammation and fibrosis in C57BL/6 mice. Arch. Toxicol. 87, 1963–1973. https://doi.org/10.1007/s00204-013-1063-z.
Gurzu, I.L., Handra, C.M., Ghita, I., Otelea, M.R., 2025. Unveiling the threat of crystalline silica on the cardiovascular system. A comprehensive review of the current knowledge. Front. Cardiovasc. Med. 12, 1506846. https://doi.org/10.3389/fcvm.2025.1506846.
Ha, H., Debnath, B., Neamati, N., 2017. Role of the CXCL8-CXCR1/2 axis in cancer and inflammatory diseases. Theranostics 7, 1543–1588. https://doi.org/10.7150/thno.15625.
Hornung, V., Bauernfeind, F., Halle, A., Samstad, E.O., Kono, H., Rock, K.L., Fitzgerald, K.A., Latz, E., 2008. Silica crystals and aluminum salts activate the NALP3 inflammasome through phagosomal destabilization. Nat. Immunol. 9, 847–856. https://doi.org/10.1038/ni.1631.
Hoy, R.F., Chambers, D.C., 2020. Silica-related diseases in the modern world. Allergy 75, 2805–2817. https://doi.org/10.1111/all.14202.
Huang, B., Liu, R., Wang, P., Yuan, Z., Yang, J., Xiong, H., Zhang, N., Huang, Q., Fu, X., Sun, W., Li, L., 2020. CD8(+)CD57(+) T cells exhibit distinct features in human non-small cell lung cancer. J. Immunother. Cancer 8. https://doi.org/10.1136/jitc-2020-000639.
Huang, R., Hao, C., Wang, D., Zhao, Q., Li, C., Wang, C., Yao, W., 2021. SPP1 derived from silica-exposed macrophage exosomes triggers fibroblast transdifferentiation. Toxicol. Appl. Pharmacol. 422, 115559. https://doi.org/10.1016/j.taap.2021.115559.
Ihim, S.A., Abubakar, S.D., Zian, Z., Sasaki, T., Saffarioun, M., Maleknia, S., Azizi, G., 2022. Interleukin-18 cytokine in immunity, inflammation, and autoimmunity: biological role in induction, regulation, and treatment. Front. Immunol. 13. https://doi.org/10.3389/fimmu.2022.919973.
JRC, 2002. *Guidance Document on the Determination of Particule Size Distribution, Fibre Length and Diameter Distribution of Chemical Substances.* EUR 20268 EN. European Commission, 2002. JRC23287.
Keane, M.P., 2008. The role of chemokines and cytokines in lung fibrosis. Eur. Respir. Rev. 17, 151–156. https://doi.org/10.1183/09059180.00010908.
Konduri, V., Oyewole-Said, D., Vazquez-Perez, J., Weldon, S.A., Halpert, M.M., Levitt, J. M., Decker, W.K., 2021. CD8+CD161+ T-Cells: Cytotoxic memory cells with high therapeutic potential. Front. Immunol. 11. https://doi.org/10.3389/fimmu.2020.613204.
Kulikauskaite, J., Wack, A., 2020. Teaching old dogs new tricks? The plasticity of lung alveolar macrophage subsets. Trends Immunol. 41, 864–877. https://doi.org/10.1016/j.it.2020.08.008.
Lee, J.H., Kim, B., Jin, W.J., Kim, H.H., Ha, H., Lee, Z.H., 2017. Pathogenic roles of CXCL10 signaling through CXCR3 and TLR4 in macrophages and T cells: relevance for arthritis. Arthritis Res. Ther. 19, 163. https://doi.org/10.1186/s13075-017-1353-6.
Leinardi, R., Pavan, C., Yedavally, H., Tomatis, M., Salvati, A., Turci, F., 2020. Cytotoxicity of fractured quartz on THP-1 human macrophages: role of the membranolytic activity of quartz and phagolysosome destabilization. Arch. Toxicol. 94, 2981–2995. https://doi.org/10.1007/s00204-020-02819-x.
Leinardi, R., Longo Sanchez-Calero, C., Huaux, F., 2022. Think beyond particle cytotoxicity: when self-cellular components released after immunogenic cell death explain chronic disease development. Front Toxicol 4, 887228. https://doi.org/10.3389/ftox.2022.887228.
Leinardi, R., Pochet, A., Uwambayinema, F., Yakoub, Y., Quesniaux, V., Ryffel, B., Broz, P., Pavan, C., Huaux, F., 2023. Gasdermin D membrane pores orchestrate IL-1α secretion from necrotic macrophages after NFS-rich silica exposure. Arch. Toxicol. 97, 1001–1015. https://doi.org/10.1007/s00204-023-03463-x.
Leinardi, R., Longo Sanchez-Calero, C., Ibouraadaten, S., Uwambayinema, F., Yakoub, Y., Pavan, C., Claus, R., Lemaire, F., Ronsmans, S., Ghosh, M., et al., 2025. Dynamic biodistribution of inhaled silica particles to extrapulmonary sites: early and late translocation mechanisms with implication for particle biomonitoring. Environ. Int. 199, 109473. https://doi.org/10.1016/j.envint.2025.109473.
Leung, C.C., Yu, I.T., Chen, W., 2012. Silicosis. Lancet 379, 2008–2018. https://doi.org/10.1016/s0140-6736(12)60235-9.
Li, W., Liang, L., Liao, Q., Li, Y., Zhou, Y., 2022. CD38: an important regulator of T cell function. Biomed. Pharmacother. 153, 113395. https://doi.org/10.1016/j.biopha.2022.113395.
Liu, S., Hao, C., Bao, L., Zhao, D., Zhang, H., Hou, J., Wang, D., Chen, H., Feng, F., Yao, W., 2019. Silica particles mediate phenotypic and functional alteration of dendritic cells and induce Th2 cell polarization. Front. Immunol. 10, 787. https://doi.org/10.3389/fimmu.2019.00787.
Liu, X., Jiang, Q., Wu, P., Han, L., Zhou, P., 2023. Global incidence, prevalence and disease burden of silicosis: 30 years' overview and forecasted trends. BMC Public Health 23, 1366. https://doi.org/10.1186/s12889-023-16295-2.
Liu, T.T., Sun, H.F., Han, Y.X., Zhan, Y., Jiang, J.D., 2024. The role of inflammation in silicosis. Front. Pharmacol. 15, 1362509. https://doi.org/10.3389/fphar.2024.1362509.
Mende, R., Vincent, F.B., Kandane-Rathnayake, R., Koelmeyer, R., Lin, E., Chang, J., Hoi, A.Y., Morand, E.F., Harris, J., Lang, T., 2018. Analysis of serum interleukin (IL)-1β and IL-18 in systemic lupus erythematosus. Front. Immunol. 9. https://doi.org/10.3389/fimmu.2018.01250.
Miller, F.W., Alfredsson, L., Costenbader, K.H., Kamen, D.L., Nelson, L.M., Norris, J.M., De Roos, A.J., 2012. Epidemiology of environmental exposures and human autoimmune diseases: findings from a national institute of environmental health sciences expert panel workshop. J. Autoimmun. 39, 259–271. https://doi.org/10.1016/j.jaut.2012.05.002.
Miyata, R., van Eeden, S.F., 2011. The innate and adaptive immune response induced by alveolar macrophages exposed to ambient particulate matter. Toxicol. Appl. Pharmacol. 257, 209–226. https://doi.org/10.1016/j.taap.2011.09.007.
Nadif, R., Mintz, M., Marzec, J., Jedlicka, A., Kauffmann, F., Kleeberger, S.R., 2006. IL18 and IL18R1 polymorphisms, lung CT and fibrosis: a longitudinal study in coal miners. Eur. Respir. J. 28, 1100–1105. https://doi.org/10.1183/09031936.00031506.
Nygaard, U.C., Ulriksen, E.S., Hjertholm, H., Sonnet, F., Bølling, A.K., Andreassen, M., Husøy, T., Dirven, H., 2021. Immune cell profiles associated with measured exposure to phthalates in the Norwegian EuroMix biomonitoring study - a mass cytometry approach in toxicology. Environ. Int. 146, 106283. https://doi.org/10.1016/j.envint.2020.106283.
Pastero, L., Turci, F., Leinardi, R., Pavan, C., Monopoli, M., 2016. Synthesis of α-Quartz with controlled properties for the investigation of the molecular determinants in silica toxicology. Cryst. Growth Des. 16, 2394–2403. https://doi.org/10.1021/acs.cgd.6b00183.
Pavan, C., Fubini, B., 2017. Unveiling the variability of "Quartz Hazard" in light of recent toxicological findings. Chem. Res. Toxicol. 30, 469–485. https://doi.org/10.1021/acs.chemrestox.6b00409.
Pavan, C., Santalucia, R., Leinardi, R., Fabbiani, M., Yakoub, Y., Uwambayinema, F., Ugliengo, P., Tomatis, M., Martra, G., Turci, F., et al., 2020. Nearly free surface silanols are the critical molecular moieties that initiate the toxicity of silica particles. Proc. Natl. Acad. Sci. U. S. A. 117, 27836–27846. https://doi.org/10.1073/pnas.2008006117.
Pavan, C., Sydor, M.J., Bellomo, C., Leinardi, R., Cananà, S., Kendall, R.L., Rebba, E., Corno, M., Ugliengo, P., Mino, L., et al., 2022. Molecular recognition between membrane epitopes and nearly free surface silanols explains silica membranolytic activity. Colloids Surf. B Biointerfaces 217, 112625. https://doi.org/10.1016/j.colsurfb.2022.112625.
Pavan, C., Escolano-Casado, G., Bellomo, C., Cananà, S., Tomatis, M., Leinardi, R., Mino, L., Turci, F., 2023. Nearly free silanols drive the interaction of crystalline silica polymorphs with membranes: implications for mineral toxicity. Front. Chem. 10. https://doi.org/10.3389/fchem.2022.1092221.
Pavan, C., Leinardi, R., Benhida, A., Ibouraadaten, S., Yakoub, Y., Svd, Brule, Lison, D., Turci, F., Huaux, F., 2024. Short- and long-term pathologic responses to quartz are induced by nearly free silanols formed during crystal fracturing. Part. Fibre Toxicol. 21, 52. https://doi.org/10.1186/s12989-024-00611-8.
Pavón, E.J., Zumaquero, E., Rosal-Vela, A., Khoo, K.M., Cerezo-Wallis, D., García-Rodríguez, S., Carrascal, M., Abian, J., Graeff, R., Callejas-Rubio, J.L., et al., 2013. Increased CD38 expression in T cells and circulating anti-CD38 IgG autoantibodies differentially correlate with distinct cytokine profiles and disease activity in systemic lupus erythematosus patients. Cytokine 62, 232–243. https://doi.org/10.1016/j.cyto.2013.02.023.
Piedra-Quintero, Z.L., Wilson, Z., Nava, P., Guerau-de-Arellano, M., 2020. CD38: an immunomodulatory molecule in inflammation and autoimmunity. Front. Immunol. 11, 597959. https://doi.org/10.3389/fimmu.2020.597959.
Poland, C.A., Duffin, R., Weber, K., Dekant, W., Borm, P.J.A., 2024. Is pulmonary inflammation a valid predictor of particle induced lung pathology? The case of amorphous and crystalline silicas. Toxicol. Lett. 399, 18–30. https://doi.org/10.1016/j.toxlet.2023.07.012.
Pollard, K.M., 2020. Perspective: the lung, particles, fibers, nanomaterials, and autoimmunity. Front. Immunol. 11, 587136. https://doi.org/10.3389/fimmu.2020.587136.
Qin, X., Niu, Z., Chen, H., Hu, Y., 2024. Macrophage-derived exosomal HMGB3 regulates silica-induced pulmonary inflammation by promoting M1 macrophage polarization

and recruitment. Part. Fibre Toxicol. 21, 12. https://doi.org/10.1186/s12989-024-00568-8.
Ronsmans, S., Goeminne, P., Jerjir, N., Nowé, V., Vandebroek, E., Keirsbilck, S., Weynand, B., Hoet, P.H.M., Vanoirbeek, J.A.J., Wuyts, W.A., et al., 2022. Outbreak of silicosis in workers producing artificial stone skirting boards: a novel application of silica-based composites. Chest 162, 406–409. https://doi.org/10.1016/j.chest.2022.03.039.
Ruijter, N., Braakhuis, H., Katsumiti, A., Garriz, I.P., Carriere, M., Zanoni, I., Candalija, A., Marshall, J., Vermeulen, J., Cassee, F.R., Boyles, M., 2025. Application of in vitro pulmonary models for hazard screening of silica particles. Arch. Toxicol. 99, 4105–4130. https://doi.org/10.1007/s00204-025-04100-5.
Saarimäki, L.A., Danielsen, P.H., Knudsen, K.B., Poulsen, S.S., Halappanavar, S., Wolff, H., Kinaret, P.A.S., Greco, D., Vogel, U., 2025. Comparison of lung inflammatory and transcriptional responses in mice and rats following pulmonary exposure to a fiber paradigm-compatible and non-compatible MWCNT. Nanomaterials 15. https://doi.org/10.3390/nano15171364.
She, Y.X., Yu, Q.Y., Tang, X.X., 2021. Role of interleukins in the pathogenesis of pulmonary fibrosis. Cell Death Discov. 7, 52. https://doi.org/10.1038/s41420-021-00437-9.
Skuland, T., Låg, M., Gutleb, A.C., Brinchmann, B.C., Serchi, T., Øvrevik, J., Holme, J.A., Refsnes, M., 2020a. Pro-inflammatory effects of crystalline- and nano-sized non-crystalline silica particles in a 3D alveolar model. Part. Fibre Toxicol. 17, 13. https://doi.org/10.1186/s12989-020-00345-3.
Skuland, T., Låg, M., Gutleb, A.C., Brinchmann, B.C., Serchi, T., Øvrevik, J., Holme, J.A., Refsnes, M., 2020b. Pro-inflammatory effects of crystalline- and nano-sized non-crystalline silica particles in a 3D alveolar model. Part. Fibre Toxicol. 17, 13. https://doi.org/10.1186/s12989-020-00345-3.
Sonnet, F., Namork, E., Stylianou, E., Gaare-Olstad, I., Huse, K., Andorf, S., Mjaaland, S., Dirven, H., Nygaard, U., 2020. Reduced polyfunctional T cells and increased cellular activation markers in adult allergy patients reporting adverse reactions to food. BMC Immunol. 21, 43. https://doi.org/10.1186/s12865-020-00373-w.
Srivastava, K.D., Rom, W.N., Jagirdar, J., Yie, T.A., Gordon, T., Tchou-Wong, K.M., 2002. Crucial role of interleukin-1beta and nitric oxide synthase in silica-induced inflammation and apoptosis in mice. Am. J. Respir. Crit. Care Med. 165, 527–533. https://doi.org/10.1164/ajrccm.165.4.2106009.
Strioga, M., Pasukoniene, V., Characiejus, D., 2011. CD8+ CD28- and CD8+ CD57+ T cells and their role in health and disease. Immunology 134, 17–32. https://doi.org/10.1111/j.1365-2567.2011.03470.x.
Tran, T.A.T., Grievink, H.W., Lipinska, K., Kluft, C., Burggraaf, J., Moerland, M., Tasev, D., Malone, K.E., 2019. Whole blood assay as a model for in vitro evaluation of inflammasome activation and subsequent caspase-mediated interleukin-1 beta release. PLoS One 14, e0214999. https://doi.org/10.1371/journal.pone.0214999.
Uhrlandt, S., 2006. Silica. In: Kirk-Othmer Encyclopedia of Chemical Technology. https://doi.org/10.1002/0471238961.0914201816012020.a01.pub2.
Ussher, J.E., Bilton, M., Attwod, E., Shadwell, J., Richardson, R., de Lara, C., Mettke, E., Kurioka, A., Hansen, T.H., Klenerman, P., Willberg, C.B., 2014. CD161++ CD8+ T cells, including the MAIT cell subset, are specifically activated by IL-12+IL-18 in a TCR-independent manner. Eur. J. Immunol. 44, 195–203. https://doi.org/10.1002/eji.201343509.
Vallyathan, V., Shi, X.L., Dalal, N.S., Irr, W., Castranova, V., 1988. Generation of free radicals from freshly fractured silica dust. Potential role in acute silica-induced lung injury. Am. Rev. Respir. Dis. 138, 1213–1219. https://doi.org/10.1164/ajrccm/138.5.1213.
Weng, S., Wang, L., Rong, Y., Liu, Y., Wang, X., Guan, H., Chen, W., 2015. Effects of the interactions between dust exposure and genetic polymorphisms in Nalp3, Caspase-1, and IL-1β on the risk of silicosis: a case-control study. PLoS One 10, e0140952. https://doi.org/10.1371/journal.pone.0140952.
Yang, Y.L., Li, X.F., Song, B., Wu, S., Wu, Y.Y., Huang, C., Li, J., 2023. The role of CCL3 in the pathogenesis of rheumatoid arthritis. Rheumatol Ther 10, 793–808. https://doi.org/10.1007/s40744-023-00554-0.
Zeidler, J.D., Hogan, K.A., Agorrody, G., Peclat, T.R., Kashyap, S., Kanamori, K.S., Gomez, L.S., Mazdeh, D.Z., Warner, G.M., Thompson, K.L., et al., 2022. The CD38 glycohydrolase and the NAD sink: implications for pathological conditions. Am J Physiol Cell Physiol 322, C521–c545. https://doi.org/10.1152/ajpcell.00451.2021.
Zhou, R., Yazdi, A.S., Menu, P., Tschopp, J., 2011. A role for mitochondria in NLRP3 inflammasome activation. Nature 469, 221–225. https://doi.org/10.1038/nature09663.
GBD, Causes of Death Collaborators, 2017. Global, regional, and national age-sex-specific mortality for 282 causes of death in 195 countries and territories, 1980-2017: a systematic analysis for the global burden of disease study 2017. Lancet 392, 1736–1788. doi:10.1016/s0140-6736(18)32203-7.